Methods for the quick analysis of micro-chaos

Gergely Gyebrószki, Gábor Csernák

1 Introduction

Chaotic vibrations arising due to the digital effects in control are well known for the last 20 years [5], [3]. Sampling and delay are commonly taken into account in control problems, however, rounding is usually neglected. It has been shown [5], [4], that rounding leads to small amplitude chaotic oscillations – referred to as *micro-chaos* because of the small amplitude – where several disconnected attractors may co-exist. In a couple of cases (inverted pendulum stabilized with D-control without delay [5], D-control with delay [1] and PD-control without delay [2]), it has been rigorously proven, that the vibrations are indeed chaotic. In [2], the coexistence of chaotic attractors were already shown. Since chaotic behaviour is generally found in theoretical models of digitally controlled systems, in this paper we are focusing on numerical methods to characterize and examine chaotic behaviour. Section 2 introduces the digitally controlled inverted pendulum – as the subject of chaos-investigation – while in Section 3 we give a short overview of methods used for characterizing chaotic behaviour. Section 4 shows different scenarios to select the region of interest for numerical methods. Section 5 is devoted to describe the Simple Cell Mapping (SCM) method and other supporting methods (such as fractal dimension calculation) for investigating chaotic behaviour and shows the SCM results for various parameters.

Gergely Gyebrószki
Budapest University of Technology and Economics, Department of Applied Mechanics, H-1111 Budapest, Műegyetem rkp 5., e-mail: gyebro@mm.bme.hu

Gábor Csernák
HAS-BUTE Research Group on Dynamics of Machines and Vehicles, H-1111 Budapest, Műegyetem rkp 5., e-mail: csernak@mm.bme.hu

2 System under examination

The *pendulum-on-a-cart* is one of the simplest devices used for demonstrating control problems. Neglecting the cart part of this device leads to a simple inverted pendulum with control. In this section, the equation of motion of the digitally controlled inverted pendulum is presented and the derivation of the so-called *micro-chaos map* is shown. The map corresponding to the inverted pendulum is used to illustrate the application of numerical methods described in the next section.

2.1 Inverted pendulum with damping and PD control

Consider an inverted pendulum with damping and digitally implemented PD control with zero order hold (i.e. the control torque is kept constant between two successive sampling instants) as shown in Fig 1. The actuator (the neglected cart) is considered to be ideal, i.e. produces the desired control effort immediately. The equation of

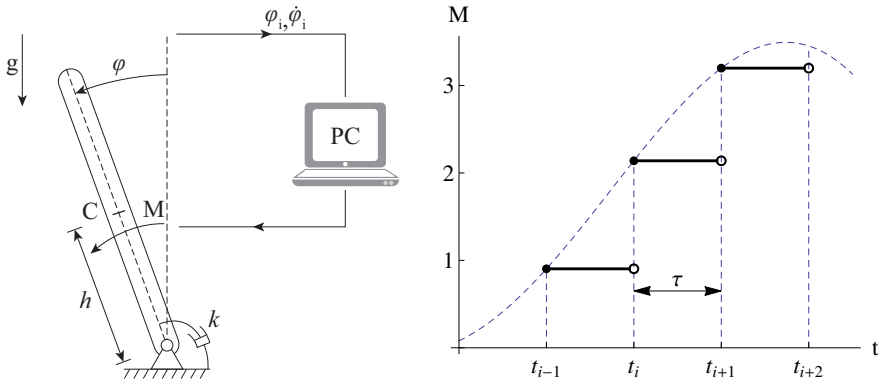

Fig. 1 The digitally controlled inverted pendulum and the control torque with respect to time.

motion of this system is

$$J\,\ddot{\varphi}(t) = mgh\sin(\varphi(t)) - k\,\dot{\varphi}(t) - p\,\varphi_i - d\,\dot{\varphi}_i, \qquad t \in [i\tau,(i+1)\tau), \tag{1}$$

where m is the mass of the pendulum, J is the mass moment of inertia about the axis of rotation, h is the distance between the centre of mass and the axis of rotation, p and d are control parameters, k is the linear damping coefficient, g is the gravitational acceleration, τ is the sampling time, while $\varphi_i = \varphi(i\tau)$ and $\dot{\varphi}_i = \dot{\varphi}(i\tau)$ are sampled values of the angular position and angular velocity respectively (at the beginning of the i-th time interval). Rearranging, linearizing and dividing (1) by J yields

$$\ddot{\varphi}(t) + 2\beta\,\dot{\varphi}(t) - \alpha^2\varphi(t) = -P\,\varphi_i - D\,\dot{\varphi}_i, \tag{2}$$

where $\alpha^2 = \frac{mgh}{J}, 2\beta = \frac{k}{J}, P = \frac{p}{J}, D = \frac{d}{J}$.
One can rewrite (2) as a system of first order differential equations:

$$\begin{aligned} \dot{\omega}(t) &= \alpha^2 \varphi(t) - 2\beta\dot{\varphi}(t) - P\varphi_i - D\omega_i, \qquad t \in [i\tau,(i+1)\tau), \\ \dot{\varphi}(t) &= \omega(t), \end{aligned} \tag{3}$$

with initial conditions: $\omega(i\tau) = \omega_i, \varphi(i\tau) = \varphi_i$.
Using the notation $\mathbf{y}_i = \left[\, \varphi(i\tau)\ \omega(i\tau) \,\right]^{\mathrm{T}}$ the solution of this equation formulates a 2D map

$$\mathbf{y}_{i+1} = (\mathbf{A} + \mathbf{B}\mathbf{K})\,\mathbf{y}_i, \qquad i \in \mathbb{N}, \tag{4}$$

where

$$\mathbf{A} = \frac{e^{-\beta\tau}}{\gamma}\begin{bmatrix} \gamma\cosh(\gamma\tau) + \beta\sinh(\gamma\tau) & \sinh(\gamma\tau) \\ \alpha^2\sinh(\gamma\tau) & \gamma\cosh(\gamma\tau) - \beta\sinh(\gamma\tau) \end{bmatrix}, \tag{5}$$

$$\mathbf{B} = \frac{e^{-\beta\tau}}{\gamma}\begin{bmatrix} \frac{\beta\sinh(\gamma\tau) + \gamma\left(\cosh(\gamma\tau) - e^{\beta\tau}\right)}{\alpha^2} \\ \sinh(\gamma\tau) \end{bmatrix}, \tag{6}$$

$$\mathbf{K} = -\left[\, P\ D \,\right], \tag{7}$$

where $\gamma = \sqrt{\alpha^2 + \beta^2}$.
Without considering rounding, one can acquire the *dimensionless form of the map*, using the notations $\hat{\alpha} = \alpha\tau, \hat{\beta} = \beta\tau, \hat{p} = P\tau^2, \hat{d} = D\tau, x = \varphi/\varphi_{\mathrm{ref}}, v = \omega/\omega_{\mathrm{ref}}$, $\hat{\mathbf{y}} = \left[\, x\ v \,\right]^T$

$$\hat{\mathbf{y}}_{i+1} = (\hat{\mathbf{A}} + \hat{\mathbf{B}}\hat{\mathbf{K}})\,\hat{\mathbf{y}}_i, \tag{8}$$

where

$$\hat{\mathbf{A}} = \frac{e^{-\hat{\beta}}}{\hat{\gamma}}\begin{bmatrix} \hat{\gamma}\cosh(\hat{\gamma}) + \hat{\beta}\sinh(\hat{\gamma}) & \sinh(\hat{\gamma}) \\ \hat{\alpha}^2\sinh(\hat{\gamma}) & \hat{\gamma}\cosh(\hat{\gamma}) - \hat{\beta}\sinh(\hat{\gamma}) \end{bmatrix}, \tag{9}$$

$$\hat{\mathbf{B}} = \frac{e^{-\hat{\beta}}}{\hat{\gamma}}\begin{bmatrix} \frac{\hat{\beta}\sinh(\hat{\gamma}) + \hat{\gamma}\left(\cosh(\hat{\gamma}) - e^{\hat{\beta}}\right)}{\alpha^2} \\ \sinh(\hat{\gamma}) \end{bmatrix}, \tag{10}$$

$$\hat{\mathbf{K}} = -\left[\, \hat{p}\ \hat{d} \,\right]. \tag{11}$$

Here $\hat{\gamma} = \sqrt{\hat{\alpha}^2 + \hat{\beta}^2}$.

2.2 Rounding at the output

Consider the case when rounding is applied to the calculated control effort (which is the output of the control system). Introducing the rounding to Equation (8) the so-called *micro-chaos map* (or μ*-chaos map*) is obtained

$$\hat{\mathbf{y}}_{i+1} = \hat{\mathbf{A}}\,\hat{\mathbf{y}}_i + \hat{\mathbf{B}}\,\mathrm{Int}(\hat{\mathbf{K}}\,\hat{\mathbf{y}}_i). \tag{12}$$

Here the reference angle in $\hat{\mathbf{y}}$ is $\varphi_{\mathrm{ref}} = r_{\mathrm{out}}\tau^2$, the reference angular velocity is $\omega_{\mathrm{ref}} = r_{\mathrm{out}}\tau$, while $r_{\mathrm{out}}\left[\frac{\mathrm{rad}}{\mathrm{s}^2}\right]$ is the resolution of the actuated control effort and $\mathrm{Int}(n)$ denotes rounding towards zero (or *truncating* or taking the integer part of n).

2.3 Rounding at the input

When rounding is applied to the measured position and velocity the corresponding form of the *micro-chaos map* is

$$\hat{\mathbf{y}}_{i+1} = \hat{\mathbf{A}}\,\hat{\mathbf{y}}_i + \hat{\mathbf{B}}\,\hat{\mathbf{K}}\,\mathrm{Int}(\hat{\mathbf{y}}_i), \tag{13}$$

where the reference angle is $\varphi_{\mathrm{ref}} = r_{\mathrm{in}}$ (i.e., the resolution of the position measurement), while the reference angular velocity is $\omega_{\mathrm{ref}} = r_{\mathrm{in}}/\tau$ since we assume that the velocity is calculated from measured position. Function $\mathrm{Int}()$ calculates the integer part of every element in the vector, returning a vector of the same dimension.

3 Numerical methods for examining chaotic behaviour

In this section the general overview of numerical methods which are useful for the quick characterization of control-related chaotic phenomena is presented. Methods are divided into two groups according to the size of region in which the chaotic behaviour is examined. The first group shows methods which are useful to characterize a single attractor, while the second group enumerates methods for examining an arbitrarily large region in the state space.

3.1 Methods for examining local chaotic behaviour

3.1.1 Iteration of the map

One can start repeatedly applying (12) – the *micro-chaos map* for the case when rounding is at the output – to a chosen initial state and will eventually find, that the iteration will not converge to a specific stable equilibrium, but after N iterations it will arrive at one of the several coexisting chaotic attractors instead. The following figures are obtained for a set of realistic parameters ($\hat{\alpha} = 6.85 \times 10^{-3}$, $\hat{\beta} = 0$, $\hat{p} = 5.5 \times 10^{-5}$, $\hat{d} = 2.5 \times 10^{-3}$) [4]. Since the number of necessary iterations N (i.e., duration of transients) is unknown, a criterion is needed to determine, whether the solution has reached an attractor. Having the exact Lyapunov exponents in hand, an

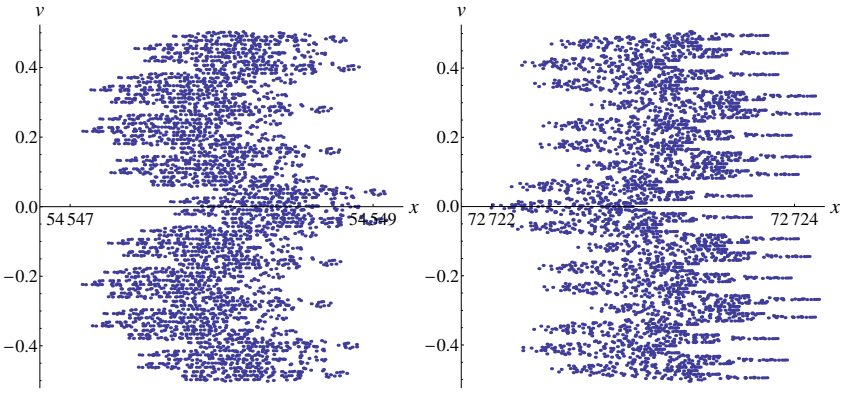

Fig. 2 Chaotic attractors when rounding is applied at the output

appropriate condition could be derived based on the time necessary for the synchronization of coupled maps used in the Lyapunov exponent estimation method [7].

3.1.2 Searching for periodic points

One can search for periodic points of the map as shown in [2]. A point $\hat{\mathbf{y}}_0$ is p-periodic if $\hat{\mathbf{y}}_p = \hat{\mathbf{y}}_0$. Groups of periodic points (periodic orbits) with high period usually correspond to the skeleton of a chaotic attractor. Consider the case, when rounding is applied to the output. Since

$$\hat{\mathbf{y}}_1 \equiv \hat{\mathbf{A}}\hat{\mathbf{y}}_0 + \hat{\mathbf{B}}\underbrace{\mathrm{Int}(\hat{\mathbf{K}}\hat{\mathbf{y}}_0)}_{:=m_1}, \tag{14}$$

$$\hat{\mathbf{y}}_2 \equiv \hat{\mathbf{A}}\hat{\mathbf{y}}_1 + \hat{\mathbf{B}}\underbrace{\mathrm{Int}(\hat{\mathbf{K}}\hat{\mathbf{y}}_1)}_{:=m_2} = \hat{\mathbf{A}}(\hat{\mathbf{A}}\hat{\mathbf{y}}_0 + \hat{\mathbf{B}}m_1) + \hat{\mathbf{B}}m_2, \tag{15}$$

$$\hat{\mathbf{y}}_p \equiv \hat{\mathbf{A}}^p\hat{\mathbf{y}}_0 + \hat{\mathbf{B}}\sum_{i=1}^{p}\hat{\mathbf{A}}^{p-i}m_i = \hat{\mathbf{y}}_0, \tag{16}$$

$$\hat{\mathbf{y}}_0 = (\mathbf{I} - \hat{\mathbf{A}}^p)^{-1}\hat{\mathbf{B}}\sum_{i=1}^{p}\hat{\mathbf{A}}^{p-i}m_i, \tag{17}$$

where m_i are integers corresponding to constant control effort. For a p-periodic orbit, checking all m_i integer combinations requires very high computational capacity. Moreover, prior to searching for periodic points, a global analysis should be performed to find specific locations of interest.

3.2 Methods for examining global chaotic behaviour

Methods mentioned in the previous subsection generally give information about a single attractor (corresponding to a specific set of initial states – i.e. the domain of attraction). However, in the case when several chaotic attractors coexist the exploration and examination of a large region of the state space is necessary.

3.2.1 Systematic iterations

Starting a set of iterations (repeatedly applying the *micro-chaos map*) from different initial states – selected either randomly or systematically in a region within the state space – one can explore the questioned region and find all attractors within it. Doing so however requires knowledge about the duration of transients or a criteria for testing whether the solution has reached an attractor. Moreover executing large number of simulations requires large computational capacity and no information on unstable equilibria can be found.

3.2.2 Cell mapping methods

Cell mapping (CM) methods are tools for the global investigation of the long term behaviour of nonlinear dynamical systems [6]. Using CM methods, periodic and chaotic solutions of the equations of motion can be found, moreover the basin of attraction can also be determined.

4 Selecting the region of interest

To obtain a global *image* of the state space, one needs to estimate the region of chaotic behaviour. This can be done using the formula for the maximal possible norm ($\mathbf{y}_\infty$) presented in [2] or the location of the attractors can be calculated based on topological assumptions.

4.1 Topological pattern

Consider the case when the rounding is applied to the output. A vector plot of (12) in case of parameters $\hat{\alpha} = 6.53 \times 10^{-3}$, $\hat{\beta} = 0$, $\hat{p} = 5.5 \times 10^{-5}$, $\hat{d} = 2.5 \times 10^{-3}$ can be seen on Fig. 3. The location of unstable fixed points can be derived from the following equation

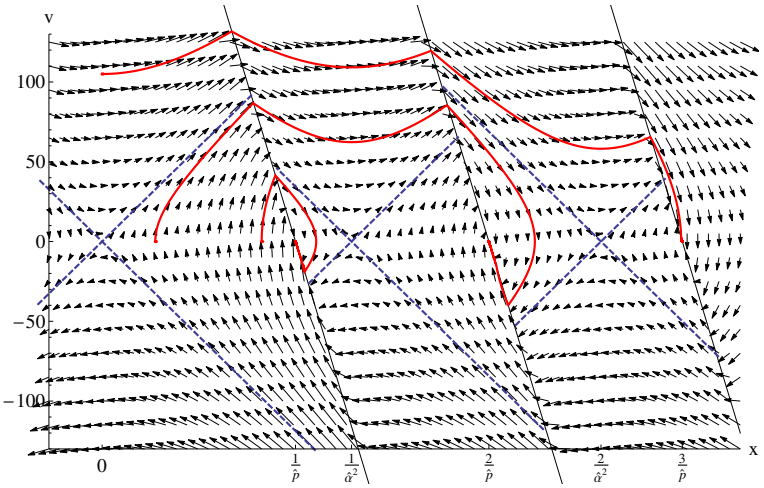

Fig. 3 Vector plot with switching lines (black lines), unstable fixed points (intersection of dashed lines) and some example trajectories leading to different attractors (curves).

$$\begin{bmatrix} x_u \\ 0 \end{bmatrix} = \hat{\mathbf{A}} \begin{bmatrix} x_u \\ 0 \end{bmatrix} + \hat{\mathbf{B}}\,\mathrm{Int}\left(\hat{\mathbf{K}} \begin{bmatrix} x_u \\ 0 \end{bmatrix}\right), \tag{18}$$

$$0 = \frac{e^{-\hat{\beta}}\sinh(\hat{\gamma})\left(\mathrm{Int}(\hat{p}\,x_u) - \hat{\alpha}^2 x_u\right)}{\hat{\gamma}}. \tag{19}$$

Since $e^{-\hat{\beta}}\sinh(\hat{\gamma})\,\hat{\gamma}^{-1} \neq 0$,

$$\mathrm{Int}(\hat{p}\,x_u) = \hat{\alpha}^2 x_u \rightarrow x_u = \frac{k}{\hat{\alpha}^2}, \qquad k \in \mathbb{Z}. \tag{20}$$

The equation of switching lines

$$\mathrm{Int}(\hat{p}\,x + \hat{d}\,v) \rightarrow v = \frac{l - \hat{p}\,x}{\hat{d}}, \qquad l \in \mathbb{Z}\backslash\{0\}. \tag{21}$$

Since dynamics of the system between two switching lines is unstable, the *stable* equilibria (i.e. attractors) are expected to be on the switching lines. The intersections between the switching lines and the x axis are:

$$x_s = \frac{l}{\hat{p}}, \qquad l \in \mathbb{Z}\backslash\{0\}. \tag{22}$$

Based on topological assumptions, the unstable fixed points and attractors should occur alternately. Since we restrict control parameters to the stable domain, $\hat{p} > \hat{\alpha}^2$, therefore the alternating pattern of unstable fixed points and attractors will end with a virtual unstable fixed point (at $l_{\max}/\hat{\alpha}^2$), thus

$$\frac{l_{\max}}{\hat{p}} < \frac{l_{\max}+1}{\hat{p}} < \frac{l_{\max}}{\hat{\alpha}^2}. \tag{23}$$

Here the first term corresponds to the location of the last attractor. See Fig. 4. The index of the last attractor is therefore:

$$l_{\max} = \mathrm{Int}\left(\frac{1}{\frac{\hat{p}}{\hat{\alpha}^2}-1}\right)+1 = \mathrm{Floor}\left(\frac{1}{\frac{\hat{p}}{\hat{\alpha}^2}-1}\right) \tag{24}$$

So the region of interest along the x axis is $x \in [-l_{\max}/\hat{p}, +l_{\max}/\hat{p}]$. The region of interest along the y axis were chosen to include the intersection of the stable manifold of the unstable fixed point in the origin and the neighbouring switching lines. One can also observe the location of unstable fixed points and *stable* attractors by plotting the left and right hand side of $\mathrm{Int}(\hat{p}\,x_u)/\hat{\alpha}^2 = x$, see Fig. 4.

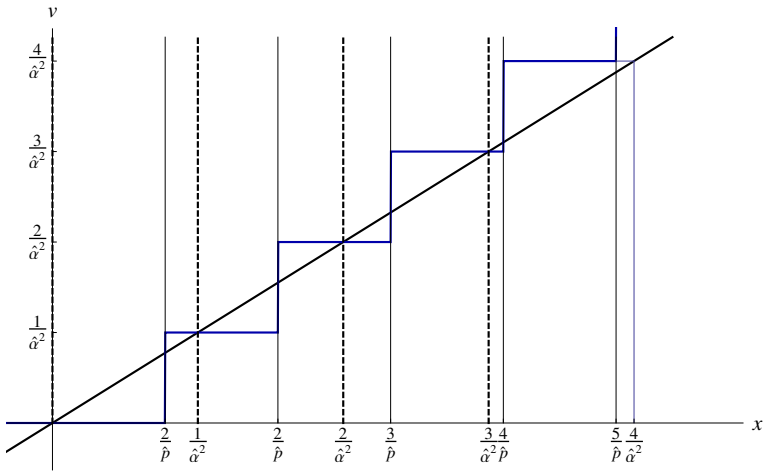

Fig. 4 Solutions of $\mathrm{Int}(\hat{p}\,x_u)/\hat{\alpha}^2 = x$ (in case of parameters $\hat{\alpha} = 6.53 \times 10^{-3}$, $\hat{p} = 5.5 \times 10^{-5}$) yielding the locations of unstable fixed points (dashed lines) and attractors (thin lines). Here $l_{\max} = 4$, the last attractor is at $l_{\max}/\hat{p}$ and the virtual unstable fixed point is at $l_{\max}/\hat{\alpha}^2$.

5 Cell mapping method and results

5.1 Simple Cell Mapping

In Simple Cell Mapping (SCM) [6], the Euclidian state space $\mathbb{R}^N$ of a dynamical system is restricted to a bounded region denoted by Ω, which is divided into M (generally rectangular) cells, indexed by $j \in \{1,..,M\}$. The region $\mathbb{R}^N \backslash \Omega$ is called

sink-cell (indexed with $j = 0$). The general idea behind SCM is that the state of the examined system is no longer described by its state vector, but with the index of the cell corresponding to that state. For each cell one or more *image cells* can be determined, where the dynamics of the system leads to. In SCM only one image cell is determined for each cell using the center point of the cell (i.e. for flows the set of ODEs describing the system are integrated for a fixed time period or for maps the map is applied to the state corresponding to the center of the cell). The image cell corresponding to cell z is denoted by $C(z)$. The mapping $z(n+1) = C(z(n))$ $C : \mathbb{N} \to \mathbb{N}$ is called a SCM and generally means, that the next state of the system is completely described by its current state (and explicitly independent of the mapping step n). In SCM, two kinds of cells are distinguished

- *periodic cells*: for which $z = C^m(z)$ is true, for $m \in \mathbb{N}$. In this case z is an m-periodic cell. If a cell z is m-periodic, cells $C(z), C^2(z), \ldots, C^{m-1}(z)$ are also m-periodic cells, and such a group of periodic cells is called an m-periodic group. By definition the sink-cell is a 1-periodic cell (once the system enters into it, it stays there forever).
- *transient cells*: which are not periodic cells. Transient cells are mapped to a periodic cell (or the sink-cell) in finite number of steps, thus representing the basin of attraction of periodic groups.

The main procedure of the SCM method is determining the type and properties of every cell. This is done by generating the sequence $C(z), C^2(z), \ldots$ (while marking cells as *visited*) for every cell z until the sequence returns to a previously visited cell. If that cell is the part of the current sequence, a new periodic group and possibly some transient cells leading to that group is found. If the cell is a previously found transient cell, the current sequence contains only transient cells leading to the same periodic group. Similarly in case the sequence leads to a previously found periodic group, all cells in the sequence are marked as transient cells leading to that group. (See the SCM algorithm in [6].) It is clear, that in the context of SCM only periodic motions occur, yet cell mapping methods are applicable for chaotic systems by taking the following assumptions stated in [6].

- Chaotic behaviour is represented by periodic groups with relatively high period.
- A chaotic attractor is represented by a set of periodic cells covering a part of the attractor in the state space.

5.2 SCM results

Some modifications were made to the SCM algorithm [6] to suit the *micro-chaos map*. Adjacent periodic groups are considered to be the part of the same attractor, therefore after the main procedure of SCM periodic groups close to each other were joined. Moreover in order to increase the precision of the method around unstable fixed points, the image cells were determined using multiple steps of the *micro-chaos map* (i.e. if the image cell of a cell was itself, the map was applied once again

– until a fixed number of repetitions – to find the image cells of cells, where the dynamics of the system is slow). This way false 1-periodic cells were eliminated.

5.2.1 Rounding at the output

When rounding is applied at the output (Section 2.2), the SCM method shows the expected topological pattern. The chaotic attractors are indeed found on the switching lines and all unstable fixed points are discovered as a set of 1-periodic cells. The area of the basin of attraction of an attractor is larger, the larger the distance of the closest neighbouring unstable fixed point is (i.e. the attractor featuring the largest basin of attraction is the one equally far away from the two neighbouring unstable fixed points). See Fig. 5. One can observe *gateways* on switching lines, which are leading to a specific chaotic attractor (See also Fig. 4.)

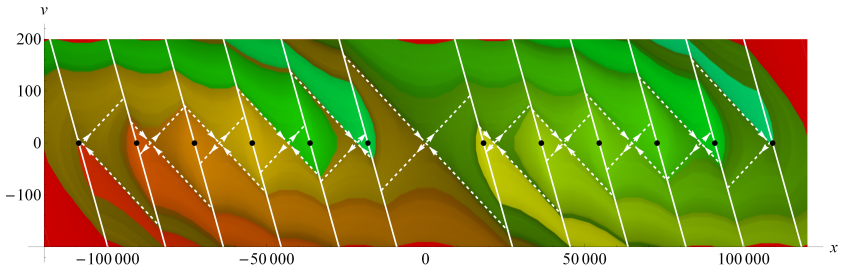

Fig. 5 SCM results with switching lines (white), stable and unstable manifolds of unstable fixed points (white, dashed) and chaotic attractors (black dots) for parameters $\hat{\alpha} = 6.8 \times 10^{-3}$, $\hat{\beta} = 0$, $\hat{p} = 5.5 \times 10^{-5}$, $\hat{d} = 2.5 \times 10^{-3}$. Here $l_{\max} = 6$, and the 3^{rd} attractor has the largest basin of attractions.

5.2.2 Effect of damping

If the damping ratio is non-zero, the eigenvectors of (9) are *rotating in clockwise direction*, therefore the previously mentioned *gateways* are moving and stretching in the direction of the y-axis.

5.2.3 Rounding at the input

In case of realistic parameters rounding at the input leads to a solution, where small amplitude chaotic motion is superposed on a periodic orbit.

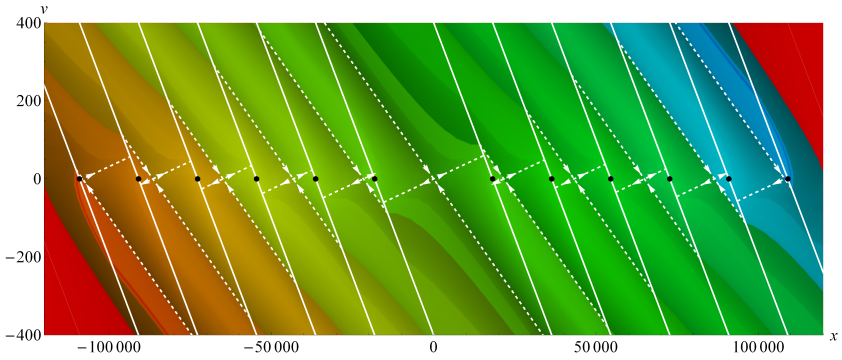

Fig. 6 SCM results for $\hat{\alpha} = 6.8 \times 10^{-3}$, $\hat{\beta} = 4.0 \times 10^{-3}$, $\hat{p} = 5.5 \times 10^{-5}$, $\hat{d} = 2.5 \times 10^{-3}$

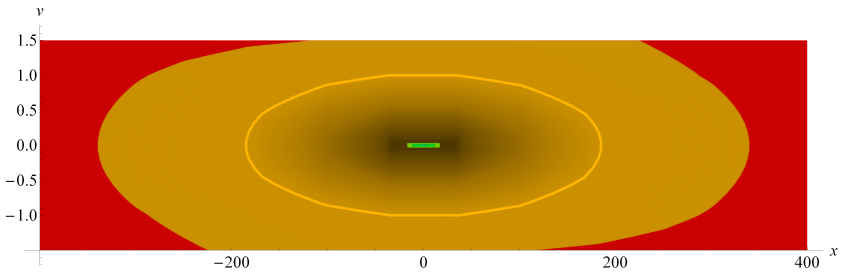

Fig. 7 SCM results for $\hat{\alpha} = 5.0 \times 10^{-3}$, $\hat{\beta} = 0$, $\hat{p} = 5.5 \times 10^{-5}$, $\hat{d} = 2.5 \times 10^{-3}$

5.2.4 Fractal dimension calculation with SCM

Since SCM utilizes rectangular cells, it could be suitable to determine the fractal dimension (*box counting* or Minkowski dimension) of chaotic attractors. SCM's with different cell sizes (ε) were applied to the close bounding region of chaotic attractors, while the total number of periodic cells $N(\varepsilon)$ were stored. Then, the box counting dimension by definition is

$$D_{\text{box}} = \lim_{\varepsilon \to 0} \frac{\log N(\varepsilon)}{\log 1/\varepsilon}. \tag{25}$$

The box counting dimension was calculated by using least squares linear regression to fit a line on $(\log 1/\varepsilon, \log N(\varepsilon))$ points. The slope of the fitted line is D_{box}. However, SCM provides greatly different images even when the cell size varies a little (Fig. 8.). Because of this phenomenon, the calculated box counting dimension will be inaccurate.

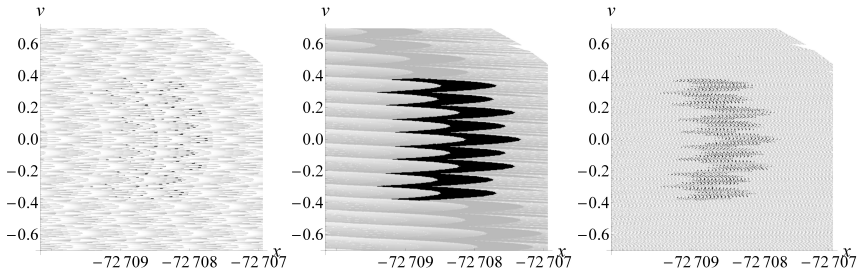

Fig. 8 SCM images of the same chaotic attractor using different cell sizes. (From left to right 940, 1100, and 1220 cells along each axis.) $\hat{\alpha} = 6.85 \times 10^{-3}$, $\hat{\beta} = 0$, $\hat{p} = 5.5 \times 10^{-5}$, $\hat{d} = 2.5 \times 10^{-3}$.

6 Conclusion

It has been shown, that Simple Cell Mapping (SCM) is a suitable tool to examine systems with complex chaotic behaviour, while it is inaccurate for box counting dimension calculation. For the case, when rounding is applied to the output (Section 2.2), the expected topological pattern was obtained by SCM and further examination of *gateways* on switching lines (defined by the stable and unstable manifolds of unstable fixed points) could help reveal unknown properties of the 2D *micro-chaos map*. On the other hand, rounding at the input (Section 2.3) shows completely different behaviour, where chaotic motion is superposed on a periodic orbit. In both cases, further investigation with more advanced CM methods is planned.

Acknowledgements This research was supported by the Hungarian National Science Foundation under grant no. OTKA K 83890.

References

1. G. Csernák, G. Stépán: Digital Control as Source of Chaotic Behavior. International Journal of Bifurcation and Chaos **20(5)**, 1365–1378 (2010)
2. G. Csernák, G. Stépán: Sampling and Round-off, as Sources of Chaos in PD-controlled Systems. Proceedings of the 19th Mediterranean Conference on Control and Automation (2011)
3. F. D. Delchamps: Stabilizing a linear system with quantized state feedback. IEEE Transactions on Automatic Control **35**, 916–924 (1990)
4. E. Enikov, G. Stépán: Micro-Chaotic Motion of Digitally Controlled Machines. Journal of Vibration and Control **4**, 427–443 (1998)
5. G. Haller, G. Stépán: Micro-Chaos in Digital Control. Journal of Nonlinear Science **6**, 415–448 (1996)
6. J. A. W. van der Spek: Cell Mapping Methods: Modifications and Extensions. Eindhoven University of Technology, Eindhoven (1994)
7. A. Stefański, T. Kapitaniak: Estimation of the dominant Lyapunov exponent of non-smooth systems on the basis of maps synchronization. Chaos, Solitons and Fractals **15**, 233–244 (2003)